Earth and Planetary Science Letters 288 (2009) 524–533

Contents lists available at ScienceDirect

Earth and Planetary Science Letters

journal homepage: www.elsevier.com/locate/epsl

Spinel–olivine magnesium isotope thermometry in the mantle and implications for the Mg isotopic composition of Earth

E.D. Young [a,b,*], E. Tonui [a], C.E. Manning [a], E. Schauble [a], C.A. Macris [a]

[a] Department of Earth and Space Sciences, 595 Charles E. Young Drive East, 2676 Geology, Los Angeles, CA 90095, USA
[b] Institute of Geophysics and Planetary Physics, University of California Los Angeles, USA

ARTICLE INFO

Article history:
Received 11 August 2009
Received in revised form 29 September 2009
Accepted 8 October 2009
Available online 4 November 2009

Editor: R.W. Carlson

Keywords:
magnesium isotopes
mantle
geochemistry
meteorites
MC-ICPMS

ABSTRACT

The magnesium isotopic composition of Earth is not yet well constrained despite significant advances in methods for measuring Mg isotope ratios in rocks. One impediment to establishing $^{25}Mg/^{24}Mg$ and $^{26}Mg/^{24}Mg$ of Earth is the lack of constraints on inter-mineral Mg isotope fractionations at high temperatures. Advances in computational chemistry afford the capacity to predict quantitatively Mg isotope fractionations among high-temperature minerals. High-precision MC-ICPMS measurements in turn provide the opportunity to test these predictions in well-characterized samples. Toward this end, we present new high-precision $^{25}Mg/^{24}Mg$ and $^{26}Mg/^{24}Mg$ measurements of mantle minerals and compare these ratios with predictions for temperature-dependent inter-mineral fractionations. Our results for two San Carlos volcanic field xenoliths show that there is measurable and systematic fractionation in Mg isotope ratios between constituent minerals that are consistent with theoretical predictions. The observed order from highest to lowest $^{25}Mg/^{24}Mg$ is spinel > clinopyroxene > orthopyroxene > olivine. The fractionation between spinel and olivine suggests an equilibration temperature of 814° +/− 60 °C based on the temperature dependence obtained from ab initio calculations. This temperature is consistent with independent *T* indicators involving spinel, suggesting that spinel and olivine are in Mg isotopic equilibrium in these mantle rocks, and lending credence to the accuracy of the results. Pyroxene, on the other hand, is apparently not in Mg isotopic equilibrium with spinel and olivine if the predicted temperature-dependent fractionations are correct. Consideration of the influences of modal abundances and inter-mineral fractionations on the Mg isotopic compositions of mantle minerals, and comparisons to new meteorite data reported herein, strengthen previous suggestions that the Earth may be different from carbonaceous chondrites in $^{25}Mg/^{24}Mg$.

1. Introduction

Isotope ratios of major rock-forming elements comprising rocky planets and asteroids can be useful tracers of planet-forming processes (Poitrasson et al., 2004; Poitrasson et al., 2005; Georg et al., 2007; Poitrasson, 2007; Weyer et al., 2007). Magnesium is an abundant rock-forming element with volatility between the most refractory elements (e.g., Al and Ca) and the moderately volatile elements (e.g., Fe) and so should prove useful as an indicator of planetary provenance. However, the magnesium isotopic composition of Earth remains poorly constrained despite recent advances in multiple-collector inductively coupled plasma-source mass spectrometry (MC-ICPMS) methods for measuring $^{25}Mg/^{24}Mg$ and $^{26}Mg/^{24}Mg$ to great precision.

One impediment to establishing $^{25}Mg/^{24}Mg$ and $^{26}Mg/^{24}Mg$ of Earth is the lack of constraints on inter-mineral Mg isotope fractionations at high temperatures. Even at magmatic or high-grade metamorphic temperatures, and in closed systems, fractionations among minerals can be sufficient to cause measurable variations in isotope ratios in a mineral as a result of differences in modal abundances (Young, 1993). The mineral olivine, for example, will be a reliable monitor of parent–body Mg isotope ratios (e.g., Norman et al., 2006) only to the extent that the effects of inter-mineral fractionations and variations in modal abundances can be removed. In addition, mineral fractionation factors provide the means to identify open-system exchange of Mg isotopes as a consequence of metasomatism, a process known to be important in mantle rocks (Rudnick and Ionov, 2007).

Advances in computational chemistry afford the capacity to predict quantitatively Mg isotope fractionations among high-temperature minerals. High-precision MC-ICPMS measurements in turn provide the opportunity to test these predictions in well-characterized samples. Toward this end, we present new high-precision $^{25}Mg/^{24}Mg$ and $^{26}Mg/^{24}Mg$ measurements of mantle minerals and compare these

* Corresponding author. Department of Earth and Space Sciences, 595 Charles E. Young Drive East, 2676 Geology, Los Angeles, CA 90095, USA.
E-mail addresses: eyoung@ess.ucla.edu (E.D. Young), eric.tonui@ucr.edu (E. Tonui), manning@ess.ucla.edu (C.E. Manning), schauble@ucla.edu (E. Schauble), cmacris@ucla.edu (C.A. Macris).

0012-821X/$ – see front matter © 2009 Elsevier B.V. All rights reserved.
doi:10.1016/j.epsl.2009.10.014

ratios with predictions for temperature-dependent inter-mineral fractionations. Results show that systematic fractionations among minerals in high-temperature rocks are resolvable and are broadly consistent with theoretical predictions. Our results confirm expectations about the order of relative enrichments in the heavier Mg isotopes as a function of Mg bonding environment. Finally, we compare our results to our new analyses of Mg isotope ratios of meteorites to address the question of whether or not Earth is chondritic in $^{25}Mg/^{24}Mg$ and $^{26}Mg/^{24}Mg$. We conclude that the Earth's mantle is higher in $^{25}Mg/^{24}Mg$ and $^{26}Mg/^{24}Mg$ than carbonaceous chondrite meteorites and thus may be "non-chondritic" in its Mg isotopic composition.

2. Samples

Two mantle xenoliths from the San Carlos ultramafic inclusion locality in southeastern Arizona, USA were sampled from a single large rock specimen (Fig. 1). One rock, CEM1-1, is a spinel harzburgite Group I xenolith (classification of Frey and Prinz, 1978) composed of 69% olivine (Ol), 28% orthopyroxene (Opx), 2.3% clinopyroxene (Cpx), and <1% chromian spinel (Spl) as determined by 1000 point analyses by electron microprobe analyzer. Representative mineral compositions, including cations per formula unit based on no vacancies, are shown in Table 1. Notable are the Cr-rich compositions of the spinel and pyroxenes and the paucity if Ti in pyroxenes.

The second xenolith, CEM1-3, is similar to the first but is a spinel lherzolite, containing less olivine and more pyroxene, with modal proportions of 62% Ol, 24% Opx, 13% Cpx, and ~1% Spl. Spinels are chromian and the overall mineral chemistry is similar to CEM1-1 (e.g., Table 1); CEM1-3 is also classified as Group I.

In addition to data for the two xenoliths, we report analyses of terrestrial and meteorite samples for comparison and context. Two samples of "San Carlos Olivine" are included in this study for comparison. One, USNM 136718, is a working standard in our laboratory. The other is a large volume of olivine from the San Carlos ultramafic site distributed by Stein Jacobsen of Harvard University. Details about the host rocks for these mantle olivines are not known. The whole-rock samples of Allende (CV3) and Orgueil (CI1) carbonaceous chondrites reported here were obtained from the Muséum National d'Histoire Naturelle, Paris, and serve as typical examples of primitive solar system materials. The samples of olivine from the two pallasite meteorites reported here, Esquel (sample no. IN 1658, oxygen isotope aliquot K) and Brenham, come from the collection at UCLA. These olivines represent differentiated early solar system material. We also report an analysis of olivine from the Apollo 17 site, sample 76335. The host rock is a troctolitic anorthosite and is regarded as a good example of primitive material from the highlands of the Moon. We report an analysis of green sand olivine sampled from the green-sand beach locality on the south side of the big island, Hawaii. The sample is taken to be representative of Kilauea basalt olivine.

Table 1
Representative mineral compositions from San Carlos xenolith CEM1-3.

Oxide (wt.%)	Spl (#5a)	Ol (#15)	Cpx (#26)	Opx (#32)
SiO_2	0.02	40.52	52.67	55.06
TiO_2	0.12	0.00	0.12	0.05
Al_2O_3	35.27	0.00	4.52	3.00
Cr_2O_3	32.81	0.02	1.44	0.62
Fe_2O_3	2.91	0.02	0.63	0.68
FeO	11.39	9.16	2.12	5.04
MnO	0.25	0.09	0.09	0.16
MgO	16.99	49.14	15.73	33.17
CaO	nd	0.06	19.65	0.76
Na_2O	nd	nd	1.65	0.13
Total	99.77	99.02	98.62	98.67
Cations per formula unit				
Si	0.000	1.000	1.928	1.924
Ti	0.003	0.000	0.003	0.001
Al	1.189	0.000	0.195	0.123
Cr	0.742	0.000	0.042	0.017
Fe^{3+}	0.063	0.000	0.017	0.018
Fe^{2+}	0.273	0.189	0.065	0.147
Mn	0.006	0.002	0.003	0.005
Mg	0.725	1.807	0.858	1.728
Ca	0.000	0.002	0.771	0.028
Na	0.000	0.000	0.117	0.008
Tot. cat.	3.000	3.000	4.000	4.000
Tot. oxy.	4.000	4.000	6.000	6.000

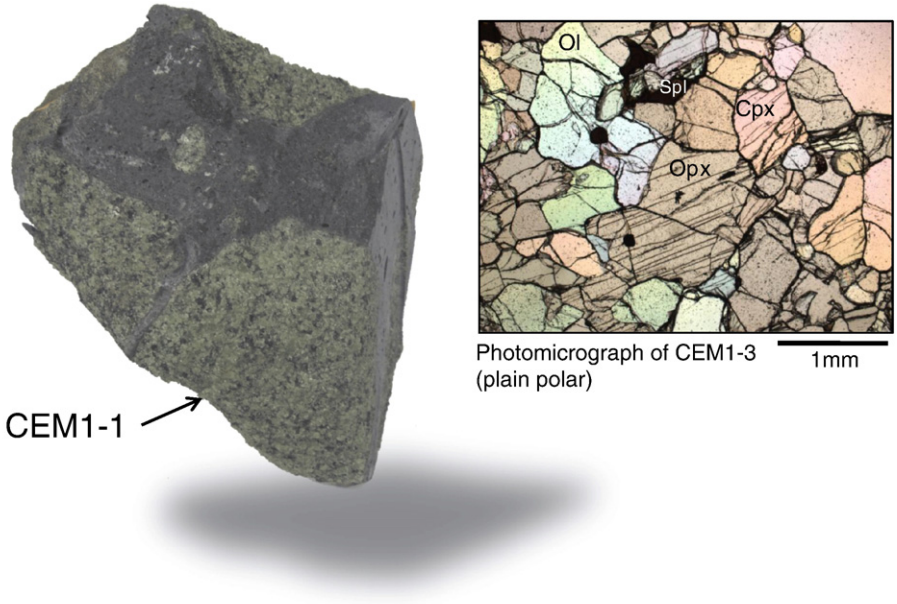

Fig. 1. Photograph of the rock specimen from the San Carlos volcanic field containing xenoliths CEM1-1 (shown) and CEM1-3 (not visible in this image). Inset shows a typical photomicrograph of CEM1-3.

3. Methods

3.1. Sample preparation and purification

Minerals were separated from the two xenoliths by handpicking with the aid of a binocular microscope. The identity of grains was confirmed by energy dispersive X-ray analysis prior to dissolution. Whole-rock samples of xenoliths consist of splits of 10 cm^3 of rock ground in an agate mortar and pestle and powdered in a tungsten carbide shatter box. Whole-rock meteorite samples represent several mg of material.

Samples were dissolved in sealed Teflon vessels jacketed in steel acid digestion bombs (Parr Instrument Co.) in a 1:1 mixture of omnigrade HF and HNO_3 at temperatures of 230 °C (e.g., for complete spinel digestion) for 72 h. Dissolved samples were transferred to high-density Teflon (Savillex™) and evaporated to dryness at 120 °C. Dried samples were dissolved again in aqua regia at 120 °C for 1 day followed by evaporation to dryness. Samples were then redissolved in 1 N HNO_3 in preparation for ion exchange column chemistry.

Magnesium was purified by ion exchange chromatography in HEPA filtered laminar flow boxes within a class 100 clean laboratory using a three-column procedure. We used PFA micro-columns measuring 120 mm × 4 mm with 70 ml reservoirs for the first two purification steps. These columns contain 1.5 ml (wet) of Bio-Rad™ AG 50W-X12 resin in 200 to 400 mesh hydrogen form. The 2.1 meq capacity of the resin translates to a column capacity of 36 mg Mg^{2+}. Columns were washed initially with 0.5 N HF followed by a rinse with ~18 MΩ cm^2/cm water, cleaning with 6 N HCl, and further rinsing. Resins were conditioned with either 1 N HNO_3 or 0.4 N HCl depending upon the application (see below). A typical load on the first column consists of between ~100 and 1000 μg of Mg in 300 μl of 1 N HNO_3. The first column is used to separate Mg from Ca, Fe, Al and Cr by eluting Mg and alkalis with 70 ml of 1 N HNO_3. Magnesium and alkalis are again evaporated to dryness. The AG 50W-X12 resins exposed to oxidizing HNO_3 were discarded after three passes. Alkalis and residual Ca are separated from Mg on the second column by loading in 300 μl of 0.4 N HCl followed by elution of alkalis with 80 ml of 0.4 N HCl. The Mg is then recovered using 65 ml of 1 N HCl. The column procedure is repeated as needed in instances where alkalis and Ca are especially abundant (not the case in the present study). Resins exposed to HCl were used time and again with no deterioration in performance. A third column is used to remove Mn. For removal of Mn we use Bio-Rad™ pre-loaded 40 mm × 8 mm columns containing AG1-X8 resin of 200 to 400 mesh size. Manganese is eluted with a 20 ml mixture of 90% ultra pure acetone and 10% 0.2 N HCl (Strelow et al., 1971) followed by Mg recovery with 6 ml of 6 N HCl.

Elution curves were determined from synthetic dissolved rock solutions containing various concentrations of Al, Mg, Ca, Fe, Cr, Mn, Fe and Ti. The most reliable indicator of complete recovery of Mg in the presence of matrix elements on the columns was the absence of measurable shifts in $^{25}Mg/^{24}Mg$ and $^{26}Mg/^{24}Mg$ following Mg recovery. These "zero enrichments" were checked for in-house reference Mg upon each load of resin. Blanks of Mg were below detection.

3.2. Mass spectrometry

All Mg isotope ratio measurements were made using a Thermo-Finnigan Neptune MC-ICPMS. The instrument has a fixed array of 9 Faraday collectors each with amplifier resistors of 10^{11} Ω. Sample purity was checked by monitoring $^{27}Al^+$, $^{44}Ca^+$, $^{56}Fe^+$, $^{52}Cr^+$, $^{55}Mn^+$ and $^{56}Fe^+$. In all cases the abundances of these potential impurities were <1 at.% of the analyte Mg concentration. Such low impurity/Mg ratios are well below thresholds for discernible matrix effects on Mg isotope ratio measurements as determined by tests using various mixtures of these elements.

Samples and standard were analyzed as ~2 ppm Mg in 2% HNO_3 aspirated through a Cetac Aridus I® desolvating nebulizer (samples were run in dry plasma) with addition of N_2. Potential mass interferences from C_2^+ and CN^+ (below detection) were resolved from $^{24}Mg^+$ and $^{26}Mg^+$, respectively, by operating at a high mass resolving power of >10,000 (m/μm as measured on the off-axis major beam peak shape). Samples were analyzed 8 to 17 times with each analysis consisting of 20 cycles of ~4 second integrations. Corrections for instrumental mass bias were obtained by sample-standard bracketing with peak height matching between sample and standard to better than 5%. Uncertainties for each datum are reported as 2 standard errors (2se), representing the uncertainty in the mean from the mass spectrometry blocks of 20 cycles.

All values for Mg isotope ratios presented in this study were obtained by using DSM3 (Galy et al., 2003) as the standard and are reported in the conventional delta notation:

$$\delta^i Mg = 10^3 \left(\frac{(^iMg/^{24}Mg)_{Sample}}{(^iMg/^{24}Mg)_{DSM3}} - 1 \right) \quad (1)$$

where i refers to 25 or 26. For completeness we also report our data using the linear form of the δ notation (Hulston and Thode, 1965) in which

$$\delta^i Mg' = 10^3 \ln \left(\frac{(^iMg/^{24}Mg)_{Sample}}{(^iMg/^{24}Mg)_{DSM3}} \right) \quad (2)$$

replaces the definition in Eq. (1). From these logarithmic delta values we calculate excesses or deficits of ^{26}Mg representing variable amounts of radiogenic ^{26}Mg, $^{26}Mg^*$, produced by decay of the short-lived nuclide ^{26}Al in the young solar system. The excesses or deficits in ^{26}Mg are characterized by the parameter $\delta^{26}Mg^* = \delta^{26}Mg' - \delta^{25}Mg'/0.511$ where 0.511 is a likely value of the exponent defining the fractionation law relating mass-dependent variations in $^{25}Mg/^{24}Mg$ to variations in $^{26}Mg/^{24}Mg$.

The aliquot of DSM3 for this work was stored as a 40 ppm concentration of Mg in a Teflon™ bottle. Potential drift in the Mg isotope ratios of the standard solution was monitored by comparing different batches of DSM3 prepared by dilution of aliquots of our stock solution (10,000 ppm in 3% HNO_3 distributed by Albert Galy, Cambridge University) over the course of the study. We find that storing solutions with Mg concentrations ≥40 ppm in Teflon bottles preserves the fidelity of the isotope ratios for timescales of years while storage in non-Teflon containers can result in drift over a period of months. As a further check on possible drift of the standard solutions we routinely analyzed two Spex CertiPrep™ Mg concentration standard solutions as internal references. The two reference solutions of 1000 ppm Mg in 2% HNO_3 are "Spex 1" (Lot# CL2-134MG) and "Spex 3" (Lot# CL3-180MG). Spex 1 has average $\delta^{25}Mg$ and $\delta^{26}Mg$ values relative to DSM3 of −1.73 +/− 0.02 (2se = $2\sigma_{mean}$, n = 5) ‰ and −3.37 +/− 0.02 (2se) ‰, respectively. Spex 3 has average $\delta^{25}Mg$ and $\delta^{26}Mg$ values relative to DSM3 of −1.04 +/− 0.01 (2se, n = 7) ‰ and −2.01 +/− 0.04 (2se) ‰, respectively. Averages of ~5 analyses of one or both of these Spex solutions during each analytical session were within uncertainties of the values quoted above.

As another accuracy check we analyzed Cambridge-1 against DSM3. Cambridge-1 is a 10,000 ppm Mg solution in 3% HNO_3 also distributed by the Cambridge laboratory. Galy et al. (2003) report $\delta^{25}Mg$ and $\delta^{26}Mg$ values of −1.33 +/− 0.07 (2σ) and −2.58 +/− 0.14 (2σ) relative to DSM3 for Cambridge-1. We received an aliquot of Cambridge-1 in 2003 and prepared (naively) a large volume of 5 ppm Mg in 2% HNO_3 stored in a non-Teflon bottle. Our $\delta^{25}Mg$ and $\delta^{26}Mg$ values relative to DSM3 at that time were −1.31 +/− 0.04‰ and −2.52 +/− 0.08‰ (2se). We measured this same 5 ppm diluted sample of Cambridge-1 in June of 2007 and obtained −1.40 +/− 0.005‰

and −2.72 +/− 0.008‰ (2se) for δ^{25}Mg and δ^{26}Mg, respectively, and measured it again in August 2008 yielding −1.40 +/− 0.005‰ and −2.71 +/− 0.07‰ (2se). We take these values to mean that our Cambridge-1 5 ppm solution was changing with time (roughly 0.002‰ per year per amu). We obtained a second aliquot of DSM3 in 2008 and confirmed that our primary DSM3 standard for this study is identical to the new aliquot. The cause of the drift in the dilute Cambridge-1 solution is unknown but most likely attributable to impurities extracted from the bottle. We have seen similar drift in other reference solutions when stored in various types of Nalgene® bottles.

For these reasons we conclude that our isotope ratio analyses presented here are accurate to better than 0.04‰ per amu relative to DSM3.

3.3. Laser ablation as a check on accuracy

We report here a single 193 nm ultraviolet laser ablation MC-ICPMS analysis of a spinel–olivine pair from xenoliths CEM1-1. Details of the protocols for our Mg isotopic analyses by laser ablation are given elsewhere (Young et al., 2005). In order to obtain laser ablation data for the Cr-bearing spinel, we needed to evaluate the effects of interferences due to Cr. We did this by noting the influence of $^{52}Cr^{++}$ on $^{26}Mg^{+}/^{24}Mg^{+}$ relative to $^{25}Mg^{+}/^{24}Mg^{+}$. The δ^{25}Mg of spinel from CEM1-1 relative to olivine in the same rock by laser ablation is 0.47 +/− 0.07 se ‰. Simple mass fractionation would predict a δ^{26}Mg value of 0.92‰ while the measured δ^{26}Mg is 1.7‰. On this basis it appears that the contribution of $^{52}Cr^{++}$ (^{52}Cr is 84% of total Cr) on δ^{26}Mg is 0.8‰ implying in turn that the influence of $^{5*}Cr^{++}$ (^{5*}Cr is 4% of total Cr) on the δ^{25}Mg values is approximately 0.04‰. The effect of Cr interference on δ^{25}Mg in the spinel is below detection with the laser method. Our reported δ^{25}Mg for the spinel by UV laser ablation MC-ICPMS is based on the measured difference between spinel and olivine and the average value for pure Mg extracted from the olivine for this rock relative to DSM3.

Laser ablation also provides us with an additional independent test of the accuracy of our solution Mg isotope ratio data. For this accuracy check we compared our acid-digestion MC-ICPMS analysis of an in-house standard with laser ablation analyses of the same standard collected over a period of several years (Table 2). The goal was to compare our results that rely on chemical purification to a method that does not rely on chemistry. The standard, referred to as P10, is a synthetic Ti and Al-rich diopside glass produced at UCLA. It has the composition $Ca_{0.97}Mg_{0.54}Si_{1.53}Al_{0.77}O_6$ based on electron microprobe analyses. We note that using a Ca-rich material for this test is especially important in view of the questions surrounding the Cpx data discussed below (Section 5.1). The acid digestion analysis was performed using the techniques described above. Measurements were made against DSM3 directly. The δ^{25}Mg value of the glass relative to DSM3 is −0.69‰ +/− 0.01 (2se). Laser ablation analyses of the glass were carried out with sample-standard bracketing to correct for instrumental fractionation. For several years in our laboratory the secondary standard for laser ablation has been the San Carlos olivine USNM 136718. The δ^{25}Mg for USNM 136718 was measured by acid digestion as part of this study (Table 2). Using this secondary standard we obtain an average laser ablation δ^{25}Mg for the P10 glass of −0.72‰ +/− 0.11 (2se). These laser ablation MC-ICPMS analyses were collected over a period from 2005 to early 2008.

We take this agreement between our independent measurements of P10, one by solution by direct comparison to DSM3, and the others by laser ablation using a sample of San Carlos olivine as the secondary standard, to mean that the accuracy of the analyses reported here is no worse than 0.1‰ and probably considerably better. This constraint on accuracy is important in view of the inter-laboratory discrepancies that persist for Mg isotope ratio analyses.

Table 2
Comparison between $^{25}Mg/^{24}Mg$ for in-house standard P10 collected by acid digestion MC-ICPMS and by laser ablation MC-ICPMS.

	$\delta^{25}Mg_{DSM3}$	2se
San Carlos Ol, USNM 136718, solution	−0.112	0.022
P10, solution (7/21/08)	−0.692	0.011
P10, LA−MC-ICPMS, $n=31$ (2005)	−0.775	0.068
P10, LA-MC-ICPMS (2/19/06)	−0.678	0.240
P10, LA-MC-ICPMS (11/11/07)	−0.693	0.107
P10, LA-MC-ICPMS (11/11/07)	−0.768	0.124
P10, LA-MC-ICPMS (11/11/07)	−0.717	0.269
P10, LA-MC-ICPMS (3/24/08)	−0.647	0.108
P10, LA-MC-ICPMS (3/24/08)	−0.703	0.108
P10, (LA-MC-ICPMS 3/24/08)	−0.813	0.109
Mean LA-MC-ICPMS P10 analyses	−0.724	
1σ	0.056	

Laser data are referenced to the acid digestion analysis of secondary standard San Carlos olivine sample USNM 136718.

Table 3
Coefficients for calculating $^{26}Mg/^{24}Mg$ fractionation between phase i and forsterite (Fo) where $10^3\ln(\alpha_{i/Fo}) = A_{i\text{-}Fo}/T^6 + B_{i\text{-}Fo}/T^4 + C_{i\text{-}Fo}/T^2 \sim \delta^{26}Mg_i - \delta^{26}Mg_{Fo}$ (Schauble, in review).

	$A_{i\text{-}Fo}$	$B_{i\text{-}Fo}$	$C_{i\text{-}Fo}$
Spinel	2.0310E+14	−1.4741E+10	9.7410E+05
Orthoenstatite	2.4820E+13	−1.8570E+09	8.3000E+04
Diopside	−1.5820E+13	2.0100E+08	1.2590E+05

3.4. Equilibrium mass-dependent Mg isotope fractionation factors

Equilibrium mass-dependent magnesium isotope fractionations were estimated thermodynamically from the lattice dynamics of ^{24}Mg- and ^{26}Mg-substituted crystals (Kieffer, 1982). The lattice dynamics models were generated using density functional perturbation theory with the gradient-corrected PBE functional and norm-conserving pseudopotentials, as implemented in the ABINIT software package (www.abinit.org) (Gonze et al., 2002). Results are expressed as $10^3\ln(\beta_{26/24})_i$ vs. temperature (T, degrees K) where for phase i

$$\beta_{26/24} = \frac{(Q_{^{26}Mg}/Q_{^{24}Mg})_i}{(Q_{^{26}Mg}/Q_{^{24}Mg})_{Mg\,gas}}. \quad (3)$$

Here Q_j is the reduced partition function for phase i composed of isotope j and Mg gas refers to the ideal gaseous Mg reference state. With this notation the $^{26}Mg/^{24}Mg$ equilibrium fractionation factor $\alpha_{i/k}$ between phases i and k is

$$\ln\alpha_{i/k} = \ln(\beta_{26/24})_i - \ln(\beta_{26/24})_k. \quad (4)$$

Table 3 shows polynomial fits of the fractionation factors between various Mg-bearing mineral phases comprising the mantle xenoliths and forsterite olivine (Fo) as a function of temperature where

$$10^3\ln(\alpha_{i/Fo}) = A_{i-Fo}/T^6 + B_{i-Fo}/T^4 + C_{i-Fo}/T^2. \quad (5)$$

Fig. 2 shows plots of $10^3\ln(\alpha_{i/Fo})$ vs. temperature. The primary source for Mg isotope fractionation factors based on these calculations, including additional phases and species, will appear in a separate publication (Schauble, in review).

4. Results

The results from this study are summarized in Table 4 and Fig. 3. In describing our results we will refer to δ^{25}Mg relative to DSM3. We use δ^{25}Mg rather than δ^{26}Mg as a general practice because when working with chondrite meteorites there is a small excess in δ^{26}Mg due to the former presence of ^{26}Al in the early solar system that in principle, though not always in practice, introduces ambiguity when comparing

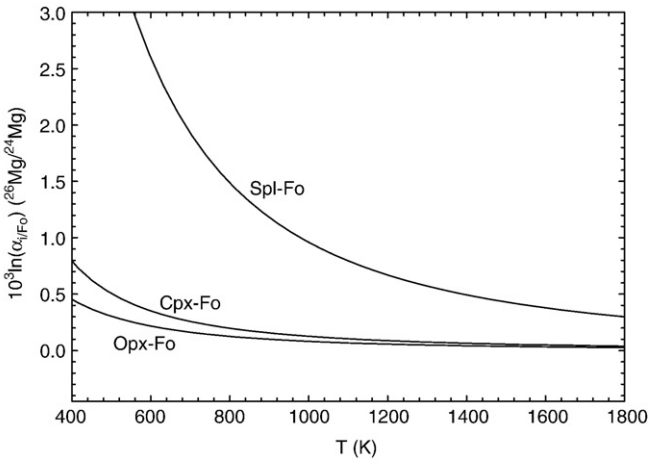

Fig. 2. Plot showing the calculated temperature dependence of δ^{26}Mg of spinel (Spl), clinopyroxene (Cpx) and orthopyroxene (Opx) relative to forsterite (Fo) expressed as $10^3\ln(\alpha_{i/Fo}) \sim \delta^{26}Mg_i - \delta^{26}Mg_{Fo}$ (Schauble, in review). The curves are calculated from the coefficients in Table 3.

terrestrial and extraterrestrial samples. We use δ^{26}Mg when discussing thermometry (Section 5.1) because the calculations are cast in terms of ^{26}Mg/^{24}Mg and we don't wish to inject ambiguity by adopting a particular mass fractionation law.

Analyses of whole-rock samples of the carbonaceous chondrites Allende (CV3) and Orgueil (CI1) have the lowest δ^{25}Mg values measured as part of this study with values of −0.21 and −0.19‰, respectively. This result is similar to most previously reported measurements of Allende and Orgueil rock (~average of −0.16‰, Table 4) but dissimilar to some others that were nearer 0.0‰ (Table 4). The latter analyses of Orgueil whole rock (Young and Galy, 2004) had led to the conclusion that DSM3 and "chondritic" are synonymous. We conclude that chondrite meteorites are not generally 0 on the DSM3 scale. The fact that primitive solar system materials are lower in δ^{25}Mg than DSM3 is supported by the −0.16‰ values for the two analyses of pallasite olivine (Table 4, Fig. 3) that represent primitive but differentiated silicate.

Olivines from the lunar highlands and from Kilauea basalt are similar to pallasite olivine with δ^{25}Mg values of −0.15 with a range of +/−0.02‰. The two samples of "San Carlos olivine" are also similar to pallasite, lunar highlands, and terrestrial basalt olivine. All of the olivines of igneous origin that we have measured have a narrow range of δ^{25}Mg values between about −0.18 and −0.13‰ (Fig. 3).

Olivines from the two San Carlos type I xenoliths are no exception to the above and are in the same range as the other igneous olivines with δ^{25}Mg values of −0.12 +/− 0.04 (1σ) and −0.17 +/− 0.01 (1σ) for CEM1-1 (harzburgite) and CEM1-3 (lherzolite), respectively. Pyroxenes are higher in δ^{25}Mg than olivine. Clinopyroxene from CEM1-1 has δ^{25}Mg = +0.10 +/− 0.03‰. Clinopyroxene from CEM1-3 is similarly high with δ^{25}Mg = +0.05 +/− 0.02 (2se) ‰ while opx from CEM1-3 is somewhat lower but still greater than olivine with δ^{25}Mg = −0.07 +/− 0.014 (2se) ‰ (Table 4, Fig. 3). In both rocks spinels have the greatest δ^{25}Mg values, with δ^{25}Mg = +0.34 +/− 0.01 (1σ) ‰ and +0.23 +/− 0.01 (1σ) ‰ for spinel in CEM1-1 and CEM1-3, respectively. The observed δ^{25}Mg values have a consistent inter-mineral variation with spinel > clinopyroxene > orthopyroxene (CEM1-3 only) > olivine. The significance of these fractionations will be discussed in Section 5.

Whole-rock samples of xenoliths CEM1-1 and CEM1-3 yield δ^{25}Mg values of −0.11 +/− 0.02 (2se) and −0.15 +/− 0.03 (2se) ‰. For CEM1-3 we have Mg isotope data for all of the major constituents. These complimentary data provide checks for internal consistency; the whole-rock δ^{25}Mg value should reflect the δ^{25}Mg values of the constituent minerals. This comparison is discussed in Section 5.

5. Discussion

5.1. Inter-mineral fractionation

The observation that δ^{25}Mg spinel > δ^{25}Mg pyroxene > δ^{25}Mg olivine is consistent with our understanding of the bonding environment of Mg in these minerals. Heavy isotopes are concentrated where vibrational frequencies of bonds are greatest, and to first order vibrational frequency ν_j for mode j depends on reduced mass μ and the force constant of the bond $K_{f,j}$

$$\nu_j = \frac{1}{2\pi}\sqrt{\frac{K_{f,j}}{\mu}}. \tag{6}$$

Expanding this concept to a summation over all force constants that affect the motions of the atoms of interest results in a simplified expression for the fractionation factor α_{a-b} between two minerals a and b applicable at high temperatures (e.g., Urey, 1947; Young et al., 2002):

$$\delta^{26}Mg_a - \delta^{26}Mg_b \cong 10^3 \ln \alpha_{a/b}^{26/24} = \frac{10^3}{24}\left(\frac{h}{k_b T}\right)^2\left(\frac{1}{m_{24}} - \frac{1}{m_{26}}\right) \times \left[\sum_j \frac{K_{f,j,a}}{4\pi^2} - \sum_j \frac{K_{f,j,b}}{4\pi^2}\right] \tag{7}$$

where m_{24} and m_{26} are the atomic masses of ^{24}Mg and ^{26}Mg, respectively, k_b is Boltzmann's constant, h is Planck's constant, and the summations are over force constants relevant to the displacements of the atoms of interest. Eq. (7) shows clearly that the heavy isotopes will be concentrated in the phases with the greater K_f.

Qualitative (and in some cases semi-quantitative) insights into the partitioning of heavy and light isotopes between mineral phases are gained by treating K_f in Eq. (7) as electrostatic in origin (Pauling, 1960). In this case the summations in Eq. (7) are over equal numbers of distinct and relevant bond pairs. The ionic model has severe limitations. Nonetheless it is useful for rationalizing structures and site occupancies in silicates and oxide minerals (Burdett and McLarnan, 1984), and it can be equally useful in formulating expectations for isotope fractionation between phases. For this purpose we turn to the concept of the mean bond strength. Pauling (1929) defined the "mean bond strength" s_i for an ionic species i as

$$\bar{s}_i = \frac{z_i}{\upsilon_i} \tag{8}$$

where z_i is the valence of the ion and υ_i is the coordination number for the ion. The force constant for a bond between cation i (in our case Mg) and anion j (e.g., O) can be written as

$$K_{f,i,j} = \frac{\bar{s}_i\ \bar{s}_j e^2 (1-n)}{4\pi\varepsilon_o r_{ij}^3} \tag{9}$$

where ε_o is the electric constant (in this case vacuum permittivity for simplicity), e is the charge of an electron, and n is the exponent in the Born–Mayer formulation for ion repulsion (Born and Mayer, 1932). Eqs. (6), (8), and (9) yield frequencies of vibration in some silicates and oxides accurate to within ~20%. For example, for the Si^{IV}–O^{II} bond one obtains an average vibrational frequency of 1023 cm^{-1}, or $\lambda = 9.8$ μm, using an empirical value for n of 12 and an established interatomic distance r_{Si-O} of 1.59×10^{-10} m. This compares favorably with the well-known ~10 μm infrared features associated with the Si–O bond in silicates. Eqs. (7)–(9) can be used similarly to formulate intuitive expectations for isotope fractionation factors. It is important to point out, however, that although these equations are useful for rationalizing fractionations among minerals with

Table 4
Magnesium isotope ratio data from this study.

		δ^{25}Mg	2se	δ^{26}Mg	2se	δ^{25}Mg′	δ^{26}Mg′	δ^{26}Mg′*	2se
Chondrites									
Allende CV3 whole rock (Paris), May 2008		−0.203	0.011	−0.380	−0.016	−0.203	−0.380	0.017	0.014
Axtel CV3 whole rock (Paris), May 2008		−0.209	0.012	−0.406	0.022	−0.209	−0.406	0.003	0.018
	Mean	**−0.206**		**−0.393**		**−0.206**	**−0.393**	**0.010**	
	1σ	**0.004**		**0.018**		**0.004**	**0.018**	**0.010**	
Orgueil CI whole rock (Paris), May 2008		**−0.193**	**0.011**	**−0.365**	**0.022**	**−0.193**	**−0.365**	**0.012**	**0.020**
Pallasites olivine									
Ol, Esquel, UCLA IN 1658, May 2008		−0.166	0.012	−0.338	0.008	−0.166	−0.338	−0.013	0.021
Ol, Brenham, May 2008		−0.143	0.012	−0.282	0.013	−0.143	−0.282	−0.001	0.021
	Mean	**−0.155**		**−0.310**		**−0.155**	**−0.310**	**−0.007**	
	1σ	**0.016**		**0.040**		**0.016**	**0.040**	**0.008**	
Earth mantle whole rocks									
SC xenolith CEM1-1, July 2009		−0.108	0.022	−0.220	0.028	−0.108	−0.220	−0.008	0.051
SC xenolith CEM1-3, July 2009		−0.145	0.033	−0.285	0.024	−0.145	−0.285	−0.002	0.069
	Mean	**−0.126**		**−0.253**		**−0.127**	**−0.253**	**−0.005**	
	1σ	**0.026**		**0.046**				**0.004**	
Earth mantle olivines									
Ol, San Carlos (USNM 136718), June 2006		−0.112	0.022	−0.174	0.051	−0.112	−0.174	0.045	0.074
Ol, San Carlos (Harvard), May 2008		−0.108	0.012	−0.193	0.013	−0.108	−0.193	0.018	0.022
Ol, SC xenolith CEM1-1, February 07		−0.079	0.015	−0.151	0.022	−0.079	−0.151	0.004	0.028
Ol, SC xenolith CEM1-1, May 2008		−0.128	0.013	−0.240	0.026	−0.128	−0.240	0.009	0.013
Ol, SC xenolith CEM1-1, May 2008		−0.158	0.012	−0.312	0.027	−0.158	−0.312	−0.002	0.027
	Mean	**−0.122**		**−0.234**		**−0.122**	**−0.234**	**0.004**	
	1σ	**0.040**		**0.080**		**0.040**	**0.080**	**0.006**	
Ol, SC xenolith CEM1-3, August 2008		−0.178	0.010	−0.342	0.014	−0.178	−0.342	0.006	0.017
Ol, SC xenolith CEM1-3, August 2008		−0.166	0.007	−0.328	0.009	−0.166	−0.328	−0.003	0.014
	Mean	**−0.172**		**−0.335**		**−0.172**	**−0.335**	**0.002**	
	Stdev	**0.008**		**0.010**		**0.008**	**0.010**	**0.007**	
Ol, xenolith average	Mean	**−0.133**		**−0.249**		**−0.133**	**−0.249**	**0.011**	
	1σ	**0.036**		**0.079**		**0.036**	**0.079**	**0.017**	
Earth mantle pyroxene									
Cpx, SC xenolith CEM1-1, February 2007		0.117	0.012	0.207	0.022	0.117	0.207	−0.022	0.023
Cpx, SC xenolith CEM1-1, May 2008		0.079	0.015	0.115	0.025	0.079	0.115	−0.039	0.020
	Mean	**0.098**		**0.161**		**0.098**	**0.161**	**−0.031**	
	1σ	**0.027**		**0.065**		**0.027**	**0.065**	**0.012**	
Cpx, SC xenolith CEM1-3, May 2008		0.054	0.019	0.074	0.036	0.054	0.074	−0.032	0.010
Cpx, xenolith average	Mean	**0.083**		**0.132**		**0.083**	**0.132**	**−0.031**	
	1σ	**0.032**		**0.068**		**0.032**	**0.068**	**0.009**	
Opx, SC xenolith CEM1-3, May 2008		**−0.066**	**0.014**	**−0.148**	**0.064**	**−0.066**	**−0.148**	**−0.019**	**0.017**
Earth mantle spinel									
Spl, SC xenolith CEM1-1, February 2007		0.333	0.034	0.640	0.049	0.333	0.640	−0.012	0.062
Spl, SC xenolith CEM1-1, May 2008		0.342	0.012	0.658	0.029	0.342	0.658	−0.012	0.009
	Mean	**0.338**		**0.649**		**0.338**	**0.649**	**−0.012**	
	1σ	**0.007**		**0.013**		**0.007**	**0.013**	**0.000**	
Spl, SC xenolith CEM1-1, UV laser ablation, Sept. 2007		**0.352**	**0.140**						
Spl, SC xenolith CEM1-3, May, 2008		0.224	0.019	0.425	0.043	0.224	0.425	−0.014	0.019
Spl, SC xenolith CEM1-3, August, 2008		0.234	0.011	0.409	0.017	0.234	0.409	−0.049	0.019
	Mean	**0.229**		**0.417**		**0.229**	**0.417**	**−0.032**	
	1σ	**0.007**		**0.011**		**0.007**	**0.011**	**0.025**	
Spl, average, this study (excluding laser ablation)	Mean	**0.283**		**0.533**		**0.283**	**0.533**	**−0.022**	
	1σ	**0.063**		**0.134**		**0.063**	**0.134**	**0.018**	
Earth basalt olivine									
Ol, Hawaii green sand, Kilauea, Nov. 06		**−0.161**	**0.013**	**−0.336**	**0.026**	**−0.161**	**−0.336**	**−0.022**	**0.018**
Lunar minerals									
Ol, anorthositic troctolite 76335, Nov. 06		**−0.133**	**0.017**	**−0.297**	**0.029**	**−0.133**	**−0.297**	**−0.037**	**0.044**

Mean values with uncertainties or single determinations with uncertainties for sample type are shown in bold.

similar bond character, they fail in many instances when trying to compare minerals with bonds of markedly different ionicity.

Eqs. (8) and (9) show explicitly that larger values for the force constant K_f correspond to smaller coordination numbers, all else equal. Eq. (7) shows that the phase with the greater values for K_f will concentrate the heavy isotopes (in order to mitigate the greater frequencies of vibration attending larger K_f). We therefore expect an inverse relationship between δ^{25}Mg and coordination of Mg and its oxygen bond partners in silicate and oxides minerals.

In olivine, Mg is bonded to six oxygens. In other words, the Mg sites are octahedral (Mg^{VI}). Spinel, on the other hand, has the structural formula $(R^{2+}_{1-i}R^{3+}_{i})^{IV}[R^{2+}_{i}R^{3+}_{2-i}]^{VI}O^{IV}_{4}$ where R represents cation species of specified charge and i, the inversion parameter, describes the distinction between normal ($i=0$) and inverse ($i=1$) spinels. A typical formula representing spinels from CEM1 is $(Mg_{0.73}Fe^{2+}_{0.27})^{IV}(Al_{1.19}Cr_{0.74}Fe^{3+}_{0.06})^{VI}O_4$ (Table 1). These spinels are "normal", to a first order, with Mg in tetrahedral coordination (the inversion parameter i for spinels from San Carlos Group I xenoliths is

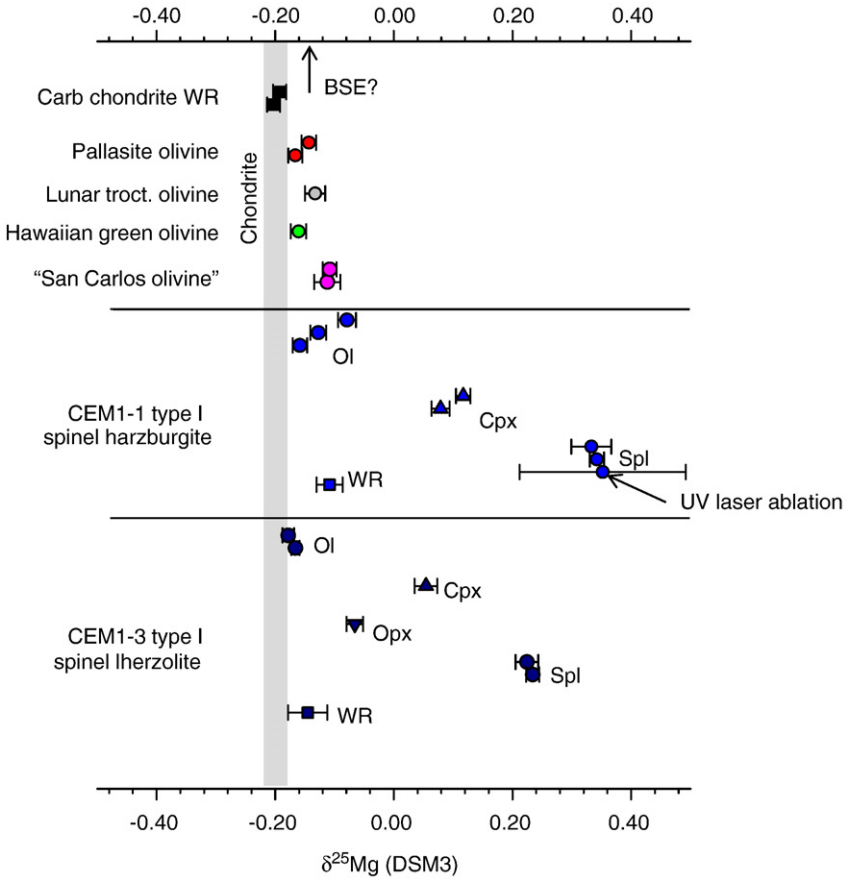

Fig. 3. Summary of δ^{25}Mg measurements relative to the DSM3 standard obtained as part of this study. The field for whole-rock chondrites is shown in grey. Error bars depict 2 standard error for each measurement. A probable value for bulk silicate Earth (BSE) based on these data is indicated.

~0.1 to 0.15, Uchida et al., 2005). Oxygen is coordinated by four cations in both olivine and spinel. Application of Eqs. (7)–(9) to the Mg^{IV}–O^{IV} bond in spinel with $r_{Mg-O} = 1.92 \times 10^{-10}$ m (e.g., Pavese et al., 2000) and the Mg^{VI}–O^{IV} bond in olivine with $r_{Mg-O} = 2.10 \times 10^{-10}$, suggests that δ^{26}Mg for spinel should be several tenths of per mil larger than that for olivine at igneous temperatures (e.g., ~0.7‰ at 1000 K). The density functional perturbation calculations quantify this expectation with rigor and confirm that spinel should have δ^{26}Mg (and δ^{25}Mg) greater than that of olivine by many tenths of per mil even at high temperatures (Table 3, Fig. 2).

The density functional theory calculations provide a quantitative estimate of Mg isotopic equilibration temperatures for the xenoliths. The observed $^{26}Mg/^{24}Mg$ fractionations between spinel and olivine for CEM1-1 and CEM1-3 are $0.88 +/- 0.08$ (1σ) and $0.75 +/- 0.02$, respectively, corresponding to temperatures of 771 °C +/− 48 (1σ) and 858 °C +/− 11, respectively. The mean is 814 °C +/− 60. These calculated Mg isotope exchange temperatures are in good agreement with the 808 °C +/− 37 obtained from X-ray diffraction studies of the inversion parameter in spinels from Group I xenoliths from San Carlos (Uchida et al., 2005). The isotope exchange temperature is approximately 200° lower than temperatures obtained from Fe^{2+}–Mg exchange between Spl, Ol and Opx in these xenoliths (O'Neill and Wall, 1987; Ballhaus et al., 1991; Liermann and Ganguly, 2003) but the latter are sensitive to estimates of Fe^{3+} in the spinel; the temperatures obtained by Fe^{2+}–Mg exchange agree with those derived from isotope exchange if there were no Fe^{3+} in Spl.

Magnesium is also in octahedral coordination in pyroxenes (the M2 site being a distorted octahedral geometry). But pyroxenes have three distinct oxygen sites. One oxygen site is in four-fold coordination (O^{IV}) and is comparable to oxygen in olivine. The other two are in three-fold coordination (O^{III}) (Ashbrook et al., 2002). As a consequence of the lower coordination of oxygen in some Mg–O bonds in pyroxene, our expectation is that pyroxenes should exhibit a greater affinity for the heavy isotopes of Mg compared with olivine. Application of Eqs. (7)–(9) to the Mg^{VI}–O^{IV} bonds in olivine and the Mg^{VI}–O^{IV} and Mg^{VI}–O^{III} bonds in pyroxenes indeed suggests that pyroxenes should exhibit the greater δ^{26}Mg (and δ^{25}Mg). The results also suggest that this difference should be much smaller than the difference between spinel and olivine (e.g., δ^{26}Mg Opx − δ^{26}Mg Ol ~ 0.2‰ at 1000 K). Here again, the detailed calculations confirm the crude expectations (Table 3, Fig. 2).

Although both pyroxene types have δ^{26}Mg (and δ^{25}Mg) values intermediate between olivine and spinel, as predicted, both clinopyroxene and orthopyroxene appear to be out of Mg isotopic equilibrium with olivine and spinel. This can be seen clearly by plotting the δ^{26}Mg fractionations between Sp, Opx, Cpx, and Ol on an isotherm plot (Fig. 4). In such a plot, minerals in isotopic equilibrium should lie along a single line with a slope defined by the equilibration temperature. In order to construct the isotherm plot, we fit the high-temperature portions of the $10^3\ln(\alpha_{i/Fo}) = A_{i\text{-}Fo}/T^6 + B_{i\text{-}Fo}/T^4 + C_{i\text{-}Fo}/T^2$ expressions to obtain a single coefficient $A'_{i\text{-}Fo}$ such that when $T > 1000$ K, $10^3\ln(\alpha_{i/Fo}) = A'_{i\text{-}Fo}/T^2$. Isotherms are then lines in plots of $10^3\ln(\alpha_{i/Fo})$ against $A'_{i\text{-}Fo}$. The isotherm plot in Fig. 4 shows that the measured Opx δ^{26}Mg values are too high to represent equilibrium with Ol and Spl based on the density functional theory calculations; the Opx–Ol fractionation suggests an equilibration temperature of ~400 °C. The measured Cpx δ^{26}Mg values also appear to be too large compared with those for Ol, with an apparent Cpx–Ol temperature of ~300 °C.

There are at least three possible explanations for the temperature discordance exhibited by the pyroxenes relative to olivine and spinel

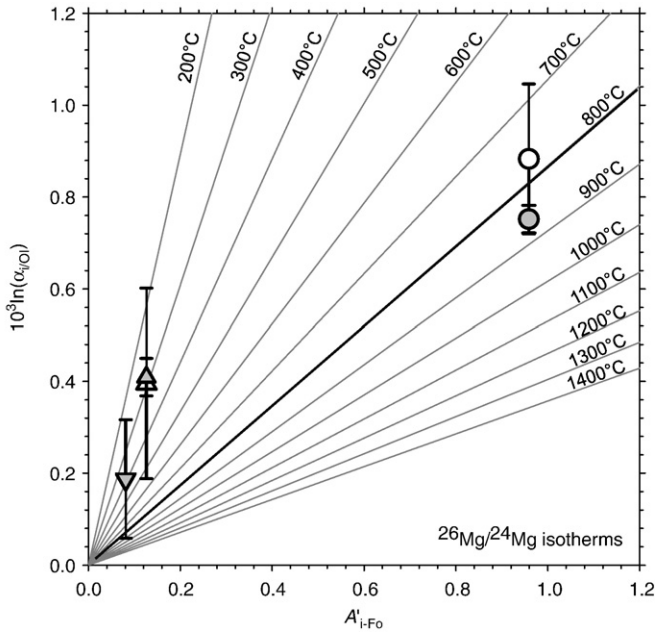

Fig. 4. Isotherm diagram showing the positions of spinel (Spl)–olivine pairs (circles), clinopyroxene (Cpx)–olivine pairs (triangles) and orthopyroxene (Opx)–olivine pairs (upside down triangles) where each pair represents $\delta^{26}Mg_i - \delta^{26}Mg_{Ol}$. The abscissa is the coefficient in the expression $10^3\ln(\alpha_{i/Fo}) = A'_{i\text{-}Fo}/T^2 \sim \delta^{26}Mg_i - \delta^{26}Mg_{Fo}$ where i is Spl, Cpx, or Opx. The coefficient $A'_{i\text{-}Fo}$ is obtained by fitting the full equations described by coefficients in Table 3 at temperatures above 1000 K. Minerals equilibrated at a single temperature are expected to lie on a single isotherm in this plot.

in CEM1-1 and CEM1-3. One possibility is that the density functional calculations are incorrect. We discount this as the sole explanation for the discordance because we can see no reason why the pyroxene calculations would be in error by such a large factor compared with calculations for olivine and spinel.

Another possibility is that the pyroxenes, especially Cpx, are not in Mg isotopic equilibrium with olivine and spinel as a result of metasomatism or exchange with a partial melt. Rudnick and Ionov (2007) found Li concentration and Li isotopic disequilibrium between Cpx and Ol in mantle xenoliths from the southeaster Siberian craton. The Cpx component in the mantle is thought to be mobile relative to Ol and Sp, for example, because it is the first major phase consumed by melting (e.g., Gudfinnsson and Presnall, 2000). Jeffcoate et al. (2007) found extensive Li isotope disequilibrium in pyroxenes, and especially in clinopyroxenes, in a San Carlos spinel lherzolite. They concluded that exchange with young interstitial melts may be the cause. Perhaps the Mg isotopes are exhibiting the same disequilibrium between Ol, Cpx and Opx that is recorded by the Li isotopes.

Lastly, it is possible that the Mg isotopic ratio analyses of the pyroxenes are in error. For example, contamination of the Cpx aliquots with Spl could raise the δ^{25}Mg values of the former. However, mass balance shows that nearly 50% of the Mg in the Cpx analyses would have to come from contaminating Spl in order to explain the data, corresponding to a volume fraction of Spl contaminant in the Cpx separate of nearly 40%. We find this unlikely as grain identities were checked by energy dispersive X-ray analysis (Section 3.1) prior to dissolution and elemental abundances were checked again in the dissolved samples. It is conceivable that spurious fractionations of Mg isotopes occurred during the purification steps for the pyroxene solutions. However, we checked our column chemistry methods for pyroxene compositions using elution curves from synthetic mixtures of Al, Mg, Ca, Fe, Cr, Mn, Fe and Ti (Section 3.1). We explore the possibility for errors in the pyroxene data and the implications of such errors in the following section.

5.2. Whole-rock $^{25}Mg/^{24}Mg$ vs. modal composition

We can explore further the issue of the discordance between pyroxenes on the one hand and olivine and spinel on the other by comparing calculated whole-rock δ^{25}Mg values with measured whole-rock δ^{25}Mg values. For this purpose we use the mass balance expression

$$\delta^{25}Mg_{WR} = 10^3\left\{\sum_i x_{Mg,i}\alpha_{i/Fo}^{25/24}\left(\frac{\delta^{25}Mg_{Ol}}{10^3}+1\right)-1\right\} \quad (10)$$

where $x_{Mg,i}$ is the fraction of the rock's Mg contained in mineral phase i, $\delta^{25}Mg_{WR}$ is the whole-rock isotopic composition, and $\alpha_{i/Fo}^{25/24} = (\alpha_{i/Fo}^{25/24})^{0.511}$as specified in Table 3 (here, in the interest of facilitating comparisons with the δ^{25}Mg data, we live with the ambiguity arising from adopting a particular relationship between the fractionation factors for $^{25}Mg/^{24}Mg$ and $^{26}Mg/^{24}Mg$). Values for $x_{Mg,i}$ come from the concentrations of Mg per formula unit in each mineral phase, $[Mg]_{PFU,i}$, as tabulated in Table 1, such that:

$$x_{Mg,i} = \frac{[Mg]_{PFU,i}(X_i/\hat{V}_i)}{\sum_j [Mg]_{PFU,j}(X_j/\hat{V}_j)}. \quad (11)$$

Here X_i is the modal fraction of mineral i in the rock and $\hat{V}_i$ is the molar volume (cm^3/mol) for the indicated mineral phase (we use 43.66, 66.20, 31.33, and 39.77 cm^3/mol for Ol, Cpx, Opx, and Spl, respectively; Berman, 1988). We can apply Eqs. (10) and (11) to CEM1-3 where we have data for all four major constituents, Ol + Cpx + Opx + Spl. Modal abundances and mineral compositions (Table 1) indicate that 63% of the Mg in CEM1-3 is in Ol, 33% is in Opx, 4% in Cpx, and 0.3% in Spl.

The modal abundances for CEM1-3, the chemical compositions of the constituent minerals, and fractionation factors at the Ol–Spl equilibrium temperature of 858 °C, yield a calculated whole-rock δ^{25}Mg of −0.127‰ relative to DSM3 that is close to the measured value of −0.145‰ +/− 0.033 (2se). The calculated whole-rock value is insensitive to plausible ranges in mineral Mg concentrations and modal abundances. For example, replacing the measured modal abundances for CEM1-3 with those for CEM1-1 (changing the volume fraction of Ol from 62% to 70%) in the calculation changes the calculated whole-rock δ^{25}Mg from −0.127 to −0.134, meaning that the calculated value is within 1se of the measured value regardless of small perturbations in modal abundance. However, we note that if we replace the measured Cpx and Opx δ^{25}Mg values with those predicted by the measured Ol δ^{25}Mg and the fractionation factors in Table 3, the calculated whole-rock δ^{25}Mg is −0.146, matching our measured value exactly. We also point out that the Cpx–Ol and Opx–Ol fractionations observed by Handler et al. (2009) are closer to, although still greater than, the predicted values. For these reasons, we cannot rule out the possibility that the Cpx δ^{25}Mg values, and possibly the Opx δ^{25}Mg values as well, are erroneously high, but neither can we demonstrate that they are spurious.

5.3. Comparisons with previous data

Our measured δ^{25}Mg values relative to DSM3 for olivine and whole rocks representing two San Carlos mantle xenoliths are in good agreement with values for mantle xenolith olivine reported by Handler et al. (2009) and Bizzarro et al. (2005). Our values are consistently ~0.1‰ lower (more negative) than those reported by Wiechert and Halliday (2007) and are ~0.2 greater (more positive) than the values reported by Teng et al. (2007) and Pearson et al. (2006). Discrepancies among the various laboratories remain unexplained. Interestingly, the same offsets between laboratories are not seen in general for CV3 chondrite meteorites.

As far as we are aware we are reporting the first $^{25}Mg/^{24}Mg$ and $^{26}Mg/^{24}Mg$ values for mantle spinels. Consistency between our measured $^{25}Mg/^{24}Mg$ fractionation between Ol and Spl and qualitative and quantitative predictions provides confidence that these inter-mineral fractionations are accurate (Fig. 5). The difference between Ol and Spl $\delta^{25}Mg$ values obtained by laser ablation MC-ICPMS is independent of solution chemistry and yet agrees with the measurements obtained by solution chemistry, suggesting that both the olivine and the spinel $\delta^{25}Mg$ values are accurate relative to DSM3.

5.4. Earth vs. chondrite

The consistency between measured inter-mineral fractionations in $^{25}Mg/^{24}Mg$ and those expected from theory can be taken as mutually reinforcing with regard to the veracity of the measurements and the theory. The agreement between acid digestion and laser ablation analyses, and the consistency between the measured mineral separate and whole rock $^{25}Mg/^{24}Mg$ values, lends further support to the assertion that the results of this study are not only precise, but accurate as well. What is more, we showed in Section 5.2 that perturbations to the whole-rock $\delta^{25}Mg$ caused by metasomatic enrichments in Cpx $^{25}Mg/^{24}Mg$ amount to no more than ~0.02‰. As a result, it is possible to draw tentative conclusions about whether or not Earth has the same $^{25}Mg/^{24}Mg$ as carbonaceous chondrites with the assumption that San Carlos xenoliths are representative of Earth's mantle.

In Fig. 6 the data from this study for carbonaceous chondrites, mantle rocks, and pallasite olivine are compared using a probability density plot. There is a resolvable difference in $\delta^{25}Mg$ of ~0.05‰ between carbonaceous chondrites on the one hand, and mantle rocks on the other. The two samples of pallasite straddle this difference. Olivines have the lowest $\delta^{25}Mg$ values among the major rock-forming minerals in mantle xenoliths, and the fact that they also have higher $\delta^{25}Mg$ values than carbonaceous chondrites is further evidence that Earth is not equivalent to carbonaceous chondrite in $^{25}Mg/^{24}Mg$. This

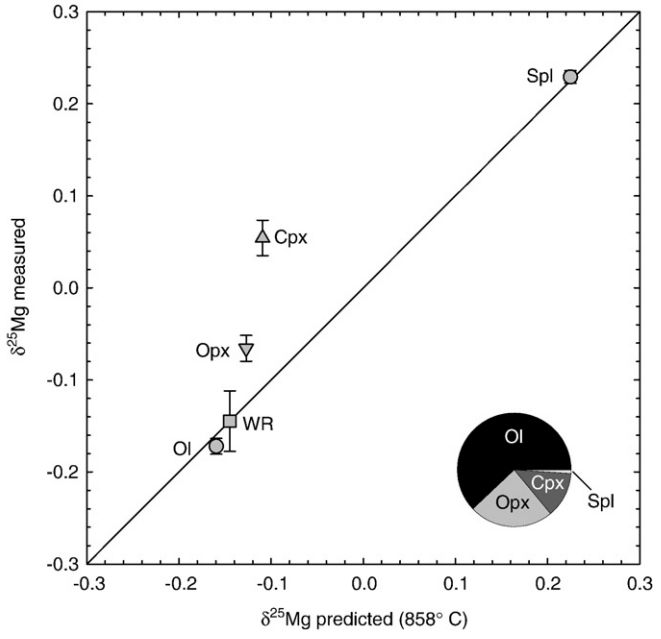

Fig. 5. Plot comparing measured $\delta^{25}Mg$ values with those predicted from inter-mineral fractionation factors at the Spl–Ol equilibration temperature and the $\delta^{25}Mg$ of the whole rock for sample CEM1-3. The 1:1 line in the figure represents mass balance if isotopic equilibrium obtains and the inter-mineral fractionation factors are accurate. The whole-rock $\delta^{25}Mg$ is by definition on the 1:1 line. Departures from the 1:1 line in the figure represent departures from equilibrium, inaccurate fractionation factors, and/or analytical errors (see text). Inset shows the relative modal abundances of olivine (Ol), clinopyroxene (Cpx), orthopyroxene (Opx) and spinel (Spl) in CEM1-3.

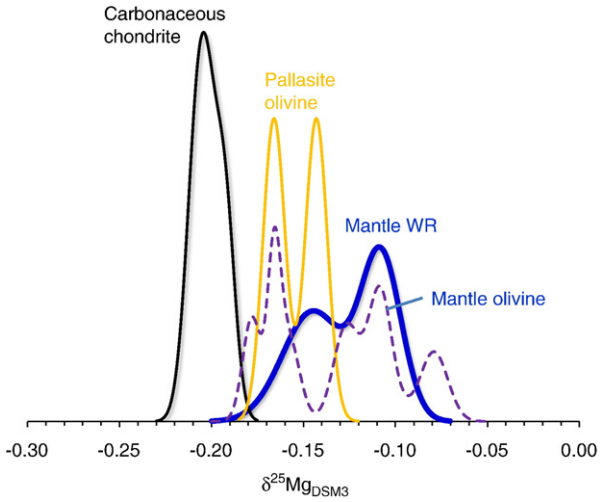

Fig. 6. Probability density plot comparing the $\delta^{25}Mg$ relative to DSM3 of carbonaceous chondrite whole rock, mantle whole rock represented by CEM1-1 and CEM1-3, mantle olivines, and olivines from pallasites as reported in this study. The plot shows a resolvable difference between differentiated rocks and carbonaceous chondrites.

conclusion is independent of the exact modal abundances in the rock, and is insensitive to the possibility of spuriously high pyroxene $\delta^{25}Mg$ values (Section 5.2). The single olivine from the lunar anorthositic troctolite is indistinguishable in $\delta^{25}Mg$ from the terrestrial mantle olivine but is clearly higher in $\delta^{25}Mg$ than the three carbonaceous chondrite rocks (Table 4), suggesting that the Moon may also be non-chondritic in $^{25}Mg/^{24}Mg$. Wiechert and Halliday (2007) had suggested previously that Earth was non-chondritic in its Mg isotope ratios. We come to the same conclusion, although our data are rather different from theirs, and comparison with more chondrite types is warranted.

Earth is also thought to have higher $^{29}Si/^{28}Si$ than chondrites (Georg et al., 2007), although the magnitude of the difference is currently debated (Fitoussi et al., 2007). The elevated $^{29}Si/^{28}Si$ may be a signature of Si dissolution into the Fe–Ni-rich core (Georg et al., 2007). It is worth considering the implications of elevated $^{25}Mg/^{24}Mg$ for Earth relative to chondrite in this context. Unlike Si, Mg is not soluble in Fe–Ni metal, and so fractionation during core formation cannot explain the high $^{25}Mg/^{24}Mg$. Because Mg and Si have similar volatilities under many conditions (e.g., Shahar and Young, 2007), a detailed analysis of the implications of a 0.05‰ enhancement in Earth's $^{25}Mg/^{24}Mg$ for $^{29}Si/^{28}Si$ may be in order. A simple conclusion to draw is that one might expect of order 0.05‰ of the $^{29}Si/^{28}Si$ excess of terrestrial rocks relative to chondrites to be associated with whatever caused the elevated $^{25}Mg/^{24}Mg$ in differentiated bodies of the solar system.

6. Conclusions

New high-precision Mg isotopic analyses of mineral separates and whole rocks representing two mantle xenoliths are compared with analyses of three carbonaceous chondrite whole rocks, olivine from two pallasites, olivine from a primitive sample of the Moon, and olivine from Kilauea. Inter-mineral $^{25}Mg/^{24}Mg$ fractionation between spinel and olivine in the mantle xenoliths is the largest yet observed in igneous rocks, but is consistent with qualitative expectations based on the different coordination of Mg in these two minerals. Agreement between results of a theoretically-derived Spl–Ol Mg isotope thermometer applied to the measured Spl–Ol fractionation and previous estimates of equilibration temperatures involving spinel in similar rocks, suggests that Spl–Ol Mg isotope fractionation could be a useful new tool in high-temperature rocks. The accuracy of the inter-mineral fractionations is verified by obtaining indistinguishable

results from laser ablation MC-ICPMS, a method that is not hostage to fractionation during chemical purification. Clinopyroxene, and to a lesser degree orthopyroxene, may be in Mg isotopic disequilibrium with respect to olivine and spinel in the xenoliths.

These new results, with accuracies affirmed by consistency in inter-mineral and whole rock measurements and independent checks by a method free of chemistry, point to a resolvable mass-dependent enrichment in ^{25}Mg and ^{26}Mg relative to ^{24}Mg compared with carbonaceous chondrites. A similar enhancement in ^{25}Mg/^{24}Mg and ^{26}Mg/^{24}Mg is seen in pallasite and lunar olivine. It appears that differentiated bodies in the solar system may be consistently high in ^{25}Mg/^{24}Mg and Mg/^{24}Mg relative to carbonaceous chondrites.

Acknowledgments

This work was supported by a grant from the NSF Division of Earth Sciences Petrology and Geochemistry program (EAR-0711411). Helpful reviews by Joel Baker and Helen Williams are most appreciated.

References

Ashbrook, S.E., Berry, A.J., Wimperis, S., 2002. ^{17}O multiple-quantum MAS NMR study of pyroxenes. J. Phys. Chem. B 2002 (106), 773–778.

Ballhaus, C., Berry, R.F., Green, D.H., 1991. High pressure experimental calibration of the olivine–orthopyroxene–spinel oxygen geobarometer: implications for the oxidation state of the upper mantle. Contrib. Mineral. Petrol. 107, 27–40.

Berman, R.G., 1988. Internally-consistent thermodynamic data for minerals in the system Na_2O–K_2O–CaO–MgO–FeO–Fe_2O_3–Al_2O_3–SiO_2–TiO_2–H_2O–CO_2. J. Petrol. 29, 445–522.

Bizzarro, M., Baker, J.A., Haack, H., Lundgaard, K.L., 2005. Rapid timescales for accretion and melting of differentiated planetesimals inferred from ^{26}Al–^{26}Mg chronometry. Astrophys. J. 632, L41–L44.

Born, M., Mayer, J.E., 1932. Z. Phys. 75 (1), 1–18.

Burdett, J.K., McLarnan, T.J., 1984. An orbital interpretation of Pauling's rules. Am. Mineral. 69, 601–621.

Fitoussi, C., Bourdon, B., Kleine, T., Reynolds, B.C., 2007. Si isotopic composition of the Earth's mantle and meteorites. American Geophysical Union Fall Meeting, U11A-0022.

Frey, F.A., Prinz, M., 1978. Ultramafic inclusions from San Carlos, Arizona: petrologic and geochemical data bearing on their petrogenesis. Earth Planet. Sci. Lett. 38, 129–176.

Galy, A., Yoffe, O., Janney, P.E., Williams, R.W., Cloquet, C., Alard, O., Halicz, L., Wadwha, M., Hutcheon, I.D., Ramon, E., Carignan, J., 2003. Magnesium isotopes heterogeneity of the isotopic standard SRM980 and new reference materials for magnesium-isotope-ratio measurements. J. Anal. At. Spectrom. 18, 1352–1356.

Georg, R.B., Halliday, A.N., Schauble, E.A., 2007. Silicon in Earth's core. Nature 447, 1102–1106.

Gonze, X., Beuken, J.-M., Caracas, R., Detraux, F., Fuchs, M., Rignanese, G.M., Sindic, L., Verstraete, M., Zerah, G., Jollet, F., Torrent, M., Roy, A., Mikami, M., Ghosez, P., Raty, J.Y., Allan, D.C., 2002. First-principles computation of material properties: the ABINIT software project. Comput. Mater. Sci. 25, 478–492.

Gudfinnsson, G.H., Presnall, D.C., 2000. Melting behaviour of model lherzolite in the system CaO–MgO–Al_2O_3–SiO_2–FeO at 0.7–2.8 GPa. J. Petrol. 41 (8), 1241–1269.

Handler, M.R., Baker, J.A., Schiller, M., Bennett, V.C., Yaxley, G.M., 2009. Magnesium stable isotope composition of Earth's upper mantle. Earth Planet. Sci. Lett. 282, 306–313.

Hulston, J.R., Thode, H.G., 1965. Variations in the S^{33}, S^{34}, and S^{36} contents of meteorites and their relation to chemical and nuclear effects. J. Geophys. Res. 70, 3475–3484.

Jeffcoate, A.B., Elliot, T., Kasemann, S.A., Ionov, D., Cooper, K., Brooker, R., 2007. Li isotope fractionation in peridotites and mafic melts. Geochim. Cosmochim. Acta 71 (1), 202–218.

Kieffer, S.W., 1982. Thermodynamics and lattice vibrations of minerals: 5. Applications to phase equilibria, isotope fractionation, and high-pressure thermodynamic properties. Rev. Geophys. Space Phys. 20, 827–849.

Liermann, H.P., Ganguly, J., 2003. Fe^{2+}–Mg fractionation between orthopyroxene and spinel: experimental calibration in the system FeO–MgO–Al_2O_3–Cr_2O_3–SiO_2, and applications. Contrib. Mineral. Petrol. 145, 217–227.

Norman, M.D., Yaxley, G.M., Bennett, V.C., Brandon, A.D., 2006. Magnesium isotopic composition of olivine from the Earth, Mars, Moon, and pallasite parent body. Geophys. Res. Lett. 33, L15202. doi:10.1029/2006GL026446.

O'Neill, H.S.C., Wall, V.J., 1987. The olivine–orthopyroxene–spinel oxygen geobarometer, the nickel precipitation curve, and the oxygen fugacity of the Earth's upper mantle. J. Petrol. 28, 1169–1191.

Pauling, L., 1929. The principles determining the structure of complex ionic crystals. J. Am. Chem. Soc. 51, 1010–1026.

Pauling, L., 1960. The Nature of the Chemical Bond. Cornell University Press.

Pavese, A., Artioli, G., Hoser, A., 2000. $MgAl_2O_4$ synthetic spinel: cation and vacancy distribution as a function of temperature, from in situ neutron powder diffraction. Z. Kristallogr. 215, 406–412.

Pearson, N.J., Griffin, W.L., Alard, O., O'Reilly, S.Y., 2006. The isotopic composition of magnesium in mantle olivine: records of depletion and metasomatism. Chem. Geol. 226, 115–133.

Poitrasson, F., 2007. Does planetary differentiation really fractionate iron isotopes? Earth Planet. Sci. Lett. 256, 484–492.

Poitrasson, F., Halliday, A.N., Lee, D.-C., Levasseur, S., Teutsch, N., 2004. Iron isotope differences between Earth, Moon, Mars and Vesta as possible records of contrasted accretion mechanisms. Earth Planet. Sci. Lett. 223, 253–266.

Poitrasson, F., Levasseur, S., Teutsch, N., 2005. Significance of iron isotope mineral fractionation in pallasites and iron meteorites for the core–mantle differentiation of terrestrial planets. Earth Planet. Sci. Lett. 234, 151–164.

Rudnick, R.L., Ionov, D.A., 2007. Lithium elemental and isotopic disequilibrium in minerals from peridotite xenoliths from far-east Russia: product of recent melt/fluid–rock reaction. Earth Planet. Sci. Lett. 256, 278–293.

Schauble, E. A., in review. First-principles estimates of equilibrium magnesium isotope fractionation in silicate, oxide, and carbonate minerals. *Geochemica et Cosmochimica Acta*.

Shahar, A., Young, E.D., 2007. Astrophysics of CAI formation as revealed by silicon isotope LA-MC-ICPMS of an igneous CAI. Earth Planet. Sci. Lett. 257, 497–510.

Strelow, F.W.E., Victor, A.H., van Zyl, C.R., Eloff, C., 1971. Distribution coefficients and cation exchange behavior of elements in hydrochloric acid-acetone. Anal. Chem. 43, 870–876.

Teng, F., Wadhwa, M., Helz, R.T., 2007. Investigation of magnesium isotope fractionation during basalt differentiation: implications for a chondritic composition of the terrestrial mantle. Earth Planet. Sci. Lett. 261, 84–92.

Uchida, H., Lavina, B., Downs, R.T., Chesley, J., 2005. Single-crystal X-ray diffraction of spinels from the San Carlos Volcanic Field, Arizona: spinel as a geothermometer. Am. Mineral. 90, 1900–1908.

Urey, H.C., 1947. The thermodynamic properties of isotopic substances. J. Chem. Soc. 562–581.

Weyer, S., Anbar, A.D., Brey, G.P., Muncker, C., Woodland, A.B., 2007. Fe-isotope fractionation during partial melting on Earth and the current view on the Fe-isotope budgets of the planets (reply to the comment of F. Poitrasson and to the comment by B.L. Beard and C.M. Johnson on "Iron isotope fractionation during planetary differentiation" by S. Weyer, A.D. Anbar, G.P. Brey, C. Munker, K. Mezger, and A.B. Woodland). Earth Planet. Sci. Lett. 256, 638–646.

Wiechert, U.H., Halliday, A.N., 2007. Non-chondritic magnesium and the origins of the inner terrestrial planets. Earth Planet. Sci. Lett. 256, 360–371.

Young, E.D., 1993. On the ^{18}O/^{16}O record of reaction progress in open and closed metamorphic systems. Earth Planet. Sci. Lett. 117, 147–167.

Young, E.D., Galy, A., 2004. The isotope geochemistry and cosmochemistry of magnesium. Geochemistry of Non-Traditional Stable Isotopes, vol. 55. MSA, pp. 197–230.

Young, E.D., Galy, A., Nagahara, H., 2002. Kinetic and equilibrium mass-dependent isotope fractionation laws in nature and their geochemical and cosmochemical significance. Geochim. Cosmochim. Acta 66 (6), 1095–1104.

Young, E.D., Simon, J.I., Galy, A., Russell, S.S., Tonui, E., Lovera, O., 2005. Supra-canonical ^{26}Al/^{27}Al and the residence time of CAIs in the solar protoplanetary disk. Science 308 (5719) Supplemental on-line material.